Ruiz, V. M., Sirera, R., Martínez, J. M. & González-Benito, J. (2020). Solution blow spun graded dielectrics based on poly(vinylidene fluoride)/multi-walled carbon nanotubes nanocomposites. *European Polymer Journal*, 122, 109397.

DOI: 10.1016/j.eurpolymj.2019.109397

Solution Blow Spun Graded Dielectrics Based on Poly(vinylidene fluoride)/Multi-walled Carbon Nanotubes Nanocomposites

À ! "#$%& '(%) *+,%- . - / 0%1 *$/ $- , %2) - 3%& '%& - $" 3/ +%34%2- 5/ $%6 #3+70' +89/ 3*#*

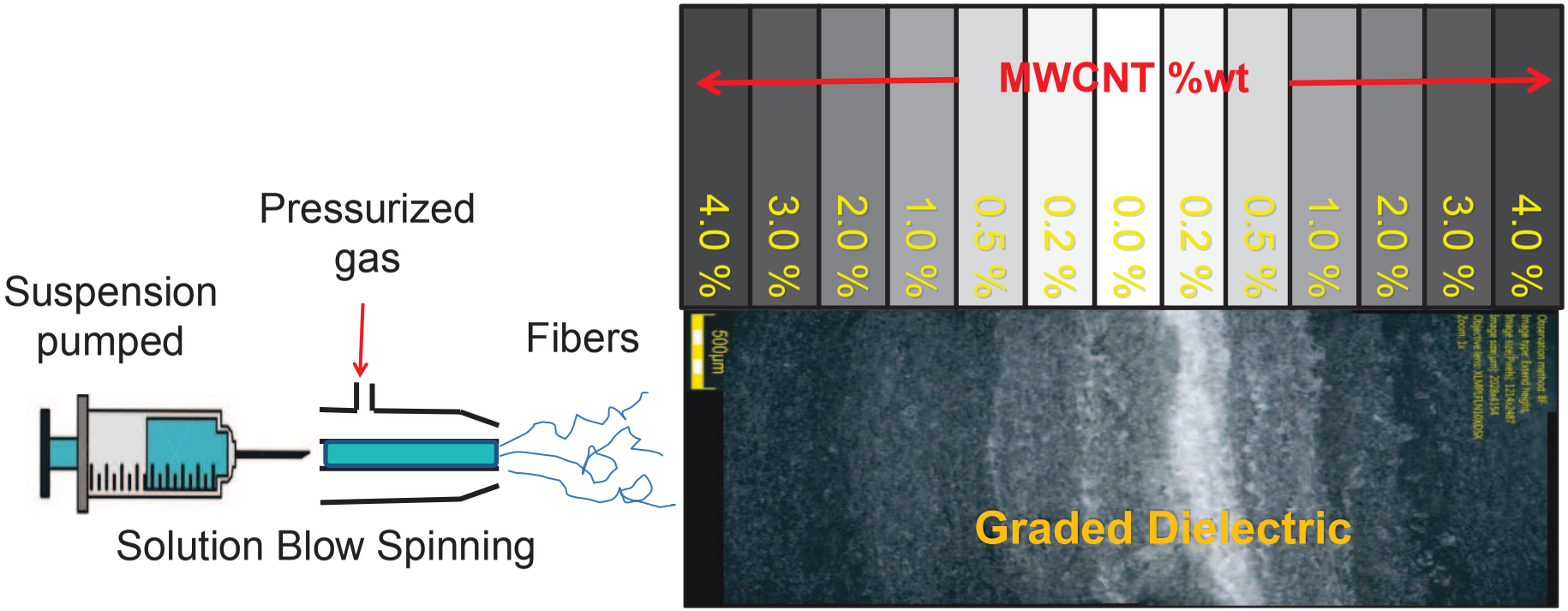

Solution Blow Spun Graded Dielectrics Based on Poly(vinylidene fluoride)/Multi-walled Carbon Nanotubes Nanocomposites

Víctor M. Ruiz[1,2], Rafael Sirera[3], Juan M. Martínez[4] and Javier González-Benito[1]*

[1]Dept. Materials Science and Engineering and Chemical Engineering, IQMAAB, Universidad Carlos III de Madrid, Madrid, Spain.

[2]Universidad Tecnológica del Centro de Veracruz, Cuitláhuac, Veracruz, México

[3]Dept. Chemistry, Universidad de Navarra, Pamplona, Spain.

[4]Dept. Electrical Engineering, DIAMAT, Universidad Carlos III de Madrid, Madrid, Spain.

[*]Corresponding author

Address: Av. Universidad 30, 28911 Leganés (Madrid – Spain)

e-mail: javid@ing.uc3m.es

ORCID iD: 0000-0002-8864-0971

Abstract

For the first time polymer-based graded nanocomposites were prepared by solution blow spinning, SBS, looking for new materials with optimal dielectric behavior. SBS was used as the processing method to apply layer by layer multi-walled carbon nanotubes, MWCNT, filled poly(vinylidene fluoride), PVDF, nanocomposites of well controlled compositions. Different configurations in terms of the disposition of layers with distinct concentration of MWCNT were considered. The structure, morphology and thermal behavior of the materials prepared were investigated so as their broadband dielectric properties in order to find and understand possible correlations. Morphological and slight structural changes were observed as a function of MWCNT concentration; however, they do not seem to be the main factors affecting the variations observed in the dielectric behavior of the materials under study. It was demonstrated that a particular design of PVDF based dielectrics, where there is a particular gradient of MWCNT concentration, importantly increases the permittivity without increasing dielectric losses.

Keywords: Nanocomposites; Functionally Graded Materials, Solution blow spinning; dielectrics.

1. Introduction

Ceramics are dielectric materials with especial applications because of their good electrical responses under different kinds of perturbations (electric, thermal, mechanical, etc). However, easier handling and processing materials are preferred for special electrical functions. In fact, many researchers are focusing their scientific interests on developing low-cost, flexible, and lightweight materials. In this sense, polymer-based materials, with high electrical sensitivities and quick dynamic responses are good candidates. If insulation of electronic components is not the final function of the material, polymers have as main disadvantage their low electric permittivity in comparison to ceramics. However, if the objective is to prepare active components (for instance, capacitors), designs focused on achieving polymer-based materials with high permittivity, ε, or easy polarizability and low dielectric losses over broadband frequency range can be optimal solutions [1].

One of the most common strategies to increase permittivity of polymers is the addition of high ε particles [2–4]. However, these materials present certain limitations; for example, they usually result in relatively low dielectric constants unless the amount of particles added is sufficiently high, above 40% by volume [4,5]. A possible improvement route is the incorporation of small amounts of conductive particles within the polymer matrix [6,7]. As consequence of an important increase of interfacial polarization, loading polymers with conductive particles near the percolation threshold may lead to high increase of permittivity [8–10]. However, although these materials may have very high permittivities they cannot be considered as good candidates for integrated capacitors due to their high dielectric losses. Different strategies have been proposed to solve this inconvenient of energy lose due to current leakage, for instance, surface modification of conducting particles [1] or use of conducting nanohybrids [11], among others. However, reducing the dielectric losses into values able to be tolerated by the capacitor together with a high permittivity is a goal not satisfied yet. Therefore, other strategies must be followed relative to materials design but in terms of higher scales. Recently, some researchers have proposed special design of materials by fabrication of multilayered dielectrics [12–14]. However, in general, they are focused on preparing materials formed by polymer dielectrics intercalated between layers of conductive particles-filled polymers for which percolation threshold is clearly overtaken.

Another interesting design of polymer composite materials looking for better dielectric performance might be achieving gradients in terms of dielectric behavior from one side to the center of the material, for example, from conducting to insulating electrical behavior, passing through semiconducting regions. As a far as the authors know, compositionally graded multilayer capacitors have been studied where each layer represent by itself a capacitor, in other words, each layer with a certain composition is separated from the others by two conductive materials (electrodes) [12–15]. In this work, preparation of compositional graded polymer-based dielectric looking for special properties is proposed. For example, layers of polymer composites with different compositions can be overlapped to prepare a material with a gradient of conductive nanoparticles content achieving high amount of particles in the outer parts and zero in the inner.

Among the existing methods of preparation of polymer-based materials solution blow spinning, SBS [16–19] might be a good candidate to prepare graded multilayer polymer composites. During SBS a polymer solution or suspension is ejected through a concentric nozzle by the action of pressurized gas to finally obtain polymer-based nonwoven fibers mats where the amount of filler can be controlled from the composition of the suspension to be blow spun [17–19]. Another possibility is the use of electrospinning, ES, from which obtaining fibers with submicrometric sizes is also possible as recent publications evidence [20,21]. Although ES has the great advantage of leading to fibers with quite good controlled sizes and even with particular orientations, its major drawback lies on the necessity of applying a relatively high electric field between the suspension dispenser and the collector. All these aspects make ES to be a processing method very difficult to scale and very complicate in order to prepare materials *in-situ*. On the contrary, SBS process, having the disadvantage of previous work to find out the best processing conditions, seems to overcome the main inconveniences of ES.

Due to its especial characteristics poly(vinylidene fluoride), PVDF, is receiving special attention for electrical applications [22]. PVDF is biocompatible, resistant against hydrolysis, abrasion and radiation and presents good mechanical strength [23]. On the other hand, PVDF may mainly appear in four different crystalline phases, α, β, γ and δ or mixtures of them [24–26]. The most stable is the α phase, the most popular is the β phase

because it can lead to the highest piezo- and pyroelectric responses and the γ phase has an intermediate electric behavior [27,28]. However, its properties highly depends on morphology and structure [27,28] which, in turn, are influenced by processing conditions [29–31] and presence of modifiers as nanofillers [26,29,32–35]. For instance, presence of carbon nanotubes CNT enhances contribution of β-phase in PVDF [18,36,37]. On the other hand, carbon nanotubes may act as nucleating agent influencing the polymer morphology [18,38,39]. Therefore, in order to understand final properties of PVDF-based composites, apart from the particular material design, the study of the influence of the presence of nanofiller in PVDF morphology and structure is a crucial prerequisite. As conductive nanoparticles carbon nanotubes are a good choice to increase permittivity of polymers by the preparation of nanocomposites because they have high aspect ratio which facilitates in addition conducting paths, reducing the percolation threshold. Besides, carbon nanotubes have high tensile strength and Young's modulus [40] which usually allows improving mechanical properties of polymers [36,41].

The aim of this work is to prepare polymer based materials with good broadband dielectric properties summarized in high permittivity and low dielectric loses to be applied in high performance capacitors. In order to prepare the materials solution blow spinning will be used to fabricate graded multilayer PVDF based materials to tune dielectric response and open novel ways of obtaining new dielectric materials with special properties. After preparing different configurations of multilayer PVDF based materials a characterization of them, in terms of morphology, structure and thermal behavior, will be carried out in order to better understand their dielectric behavior.

2. Materials and Methods

2.1. Materials

Nanocomposites were prepared by mixing poly(vinylidene fluoride), PVDF, with multi-walled carbon nanotubes, MWCNT. PVDF is a thermoplastic polymer purchased from Aldrich Chemistry (Madrid-Spain) that acted as the matrix in the composites (data given by the supplier: M_n ~ 107,000 Da; M_w ~ 275,000 Da; and density 1.78 g/mL). On the other hand, MWCNT, acting as the filler in the composites, were also purchased from Aldrich Chemistry (Madrid-Spain), which provided the following information: 95 %wt

of pure carbon, diameters ranging from 6 to 9 nm, lengths of about 5 μm and density 2.1 g/mLcm^3. Dimethylformamide, DMF (anhydrous 99.8 %), and acetone, Ac (HPLC plus, residues analysis ≥ 99.9 %) supplied by Sigma-Aldrich (Madrid-Spain) were used to prepare the solutions and suspensions to be blow spun. All materials and solvents were used as received without further purification.

2.2. Sample preparation

All samples in the form of mono or multilayer were prepared by solution blow spinning ejecting specific solutions or suspensions consecutively to fabricate layer by layer the materials. Solutions and suspensions were obtained using as liquid solvent a mixture of DMF/Ac (90% v/v of Ac). The PVDF polymer was added to the DMF/Ac liquid mixture to get in any case 10 mL of solutions and suspensions with a polymer concentration of 0.1 g/mL. To prepare the suspensions, MWCNT were firstly added to 3 mL of Ac, sonicated for 30 min at room temperature and finally, added to a solution made with 1 g of PVDF dissolved in 5 mL of a mixture DMF/Ac (1:4 v/v). To reach the final 10 mL of the suspensions to be blow spun, 2 mL more of acetone, used to recover all possible MWCNT remaining in the vial subjected to sonication, were also added to the mixture. Different concentrations of MWCNT were used to prepare the suspensions in order to obtain layers with different compositions (0%, 0.2%, 0.5%, 1%, 2%, 3% and 4% by weight of MWCNT).

The final materials were obtained by blow spinning layers in different configurations. Table 1 gathers codes and description of the different materials prepared. On the other hand, Figure 1 shows schematically the multilayer structure of the materials prepared by SBS, including some images representing circular specimens (16 mm of diameter) used to carry out the dielectric characterization.

Table 1. Codes and description of the different materials prepared.

Sample Code	**Nº of layers**	**Composition of layers (separated by dashes % wt MWCNT)**
PVDF	1	0
PVDF-0.2	3	0.2-0-0.2
PVDF-0.5		0.5-0-0.5

PVDF-1.0		1.0-0-1.0
PVDF-2.0		2.0-0-2.0
PVDF-3.0		3.0-0-3.0
PVDF-4.0		4.0-0-4.0
P5Layers	5	0.5-0.2-0-0.2-0.5
P13Layers	13	4.0-3.0-2.0-1.0-0.5-0.2-0-0.2-0.5-1.0-2.0-3.0-4.0

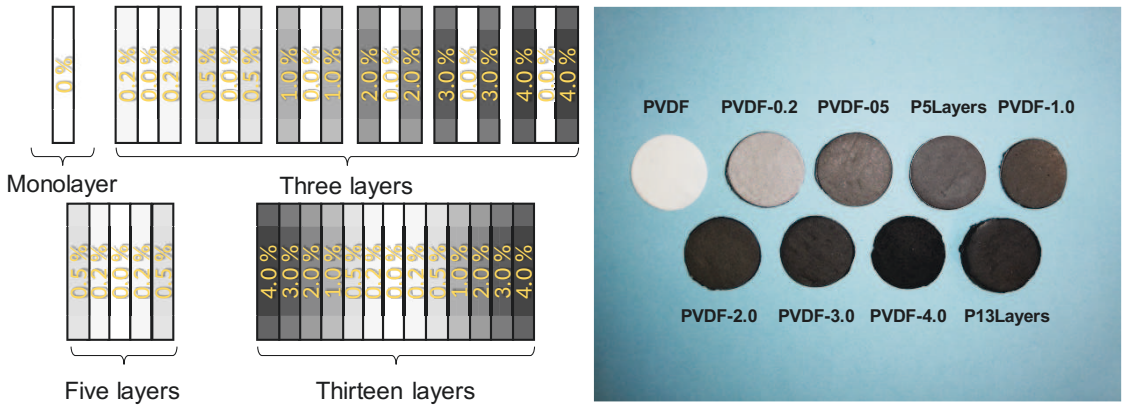

Figure 1. Scheme representing the multilayer structure of the materials prepared by SBS (left) and a photograph of representative specimens (right).

Each PVDF-based layer was obtained using a home-made SBS equipment inspired in that patented by Medeiros et al [42,43]. The SBS machine is composed by a nozzle made of aluminum (core diameter 0.7 mm) through which a glass capillary (inner diameter 0.5 mm) is passed protruding 2 mm beyond and connected to a plastic syringe coupled to an automatic pump (NE 1000 X, New Era System, Inc., Farmingdale, NY). Furthermore, an air compressor with a pressure regulator is used to supply air gas at 2 bar through an aperture in the nozzle. The mixtures were pumped at 0.5 mL/min and ejected from the nozzle to finally be deposited on a rotating cylindrical collector wrapped by aluminum foil and located at a working distance of 15 cm. In principle, the way of depositing the materials on the collector by SBS is always the same because the SBS conditions were well controlled. Therefore, similar layers thicknesses are expected to be obtained because the amount of PVDF polymer deposited per layer is fixed. Slight variations can be found due to slight extra pressure exerted over the first layers deposited.

2.3. Characterization

The multilayer PVDF-MWCNT nanocomposites were observed by an optical profilometer Opto-digital microscope OLYMPUS DSX500 (objective ×10). Samples were cut under cryogenic conditions and their cross-sections were imaged and analyzed using the Image J Software.

In order to study the morphology and composition of the different layers a TENEO field emission scanning electron microscope, FESEM (FEI) was used. The morphology was inspected by secondary and backscattered electrons using an ETD and Trinity T1 (in-lens working in the A+B Z-contrast mode) detectors, respectively. An acceleration voltage of 5 kV was applied. In order to avoid electrostatic charge accumulation they were carbon coated by evaporation using a Leica EM ACE200 low vacuum coater.

Structural characterization of the specimens were carried out by X-ray diffraction (XRD) and attenuated total reflection Fourier transformed infrared spectroscopy (ATR-FTIR). The infrared spectra were recorded in a Shimadzu IRAffinity-1S spectrometer equipped with a Golden Gate ATR accessory (diamond window), from 600 to 4000 cm^{-1} with a resolution of 4 cm^{-1} and averaging 32 scans. OMNIC 6.0 software was used to analyse the spectra. A X-ray powder diffractometer Bruker ECO D8 Advance (Bruker, Karslruhe, Germany) with a Cu $K_{\alpha 1}$ radiation were used. Patterns from 5 to 35º (2θ), 2 seconds per step, and a step size of 0.02º were collected, in a Bragg-Brentano configuration, and coupled to a detector Lynxeye XE-T. Samples were deposited onto amorphous glass in order to be measured.

Differential scanning calorimetry, DSC, was used to study the thermal behavior of the materials. Experiments were carried out with a Mettler Toledo 822e calorimeter under nitrogen atmosphere. Samples (3-4 mg) were subjected to five thermal cycles: i) a heating process from 40 to 200 ºC at 10 ºC/min; ii) an isothermal process at 200 ºC for 5 minutes to ensure that the processing and thermal history of the samples are erased; iii) a cooling process from 200 ºC to 40 ºC at 10 ºC/min; iv) an isothermal process at 40 ºC for 5 minutes and v) a second heating from 40 to 200 ºC at 10 ºC/min. From endothermic peaks and areas melting temperatures, T_m, and enthalpies of fusion, ΔH_m, were obtained while from exothermic peaks and areas crystallization temperatures, T_c, and enthalpies of crystallization, ΔH_c, were obtained. To calculate the crystallinity degrees, χ_m (SBS prepared samples) and χ_c (samples with erased processing and thermal history) the following equations were used (eq. 1).

$$\chi m = \frac{\Delta H_m}{(1-x)\cdot \Delta H_m^0}$$

$$\chi_c = \frac{\Delta H_C}{(1-x)\cdot\Delta H_m^0} \quad (1)$$

where x is the weight fraction of MWCNT and ΔH^o_m = 104.7 J/g is the standard enthalpy of fusion for the fully crystallized PVDF [44].

The electrical tests were conducted at 22 ºC and carried out using a homemade cell as that one described elsewhere [45]. The specimens were not previously metalized because the metallic coating might penetrate through the pores, which might change materials impedance response. An impedance analyzer SOLARTRON 1260A was used to carry out the impedance measurements at room temperature in the frequency range 1.0 Hz–1 MHz. A 3V amplitude sinusoidal voltage signal was applied to the specimens and the current was measured to obtain the complex impedance (real and imaginary parts, Z' and Z'' respectively) with its amplitude (ratio between peak voltage and peak current) and phase (phase between voltage and current) as a function of frequency (20 points per decade). Then the relative permittivity or dielectric constant, ε_r, and loss factor, tan δ, were estimated using well known and conventional relations (eqs. 2-4) [46].

$$\varepsilon' = \frac{Z''}{\omega C_0 (Z'^2 + Z''^2)} \quad (2)$$

$$\varepsilon'' = \frac{Z'}{\omega C_0 (Z'^2 + Z''^2)} \quad (3)$$

$$\tan\delta(\omega) = \frac{\varepsilon''}{\varepsilon'} \quad (4)$$

Where ε_0 = 8.854 ×10^{-12} F/m is the permittivity of vacuum, ε' and ε'' are the real and imaginary parts of the complex permittivity respectively and δ is the phase shift. C_0 = ε_0A/d where *A* is the electrode area in contact with the specimen and *d* the thickness of the specimen and ω = 2πf where f is the frequency in Hertz.

3. Results and Discussion

As an example in Figure 2 representative optical images of cross-sections of some of the materials schematically presented in Figure 1 (left) are shown. On the other hand, in

Figure 3 the material made of thirteen layers is depicted. As can be seen, there is a gradient in terms of darkness as a function of the concentration of carbon nanotubes. Besides, when multiple layer systems are considered it is observed that there is not homogeneity in terms of the layer thickness (Figure 2b and c and Figure 3). For all the materials prepared thickness of layers gradually increases from one side (face directly in contact with the collector) to the other. This last result might be explained simply considering that SBS process exerts certain pressure on the material causing slightly higher compaction of the first layers deposited on the collector.

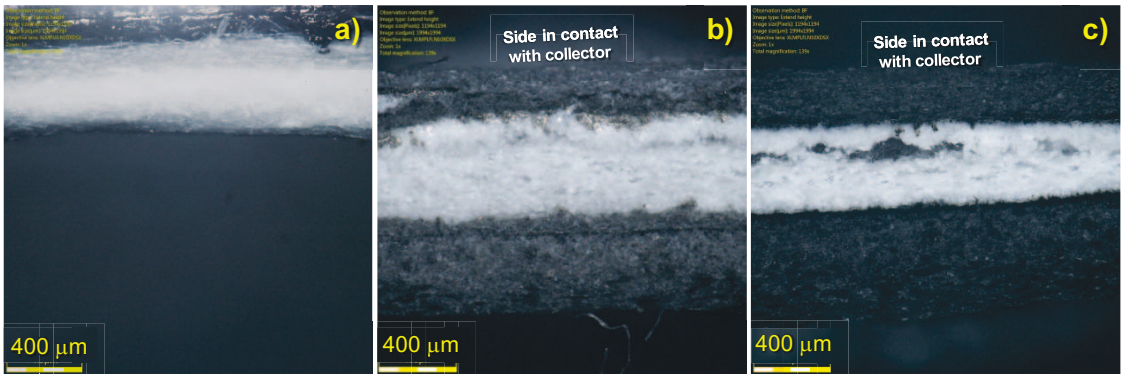

Figure 2. Representative optical images (cross-sections) of some of the materials schematically presented in Figure 1 (left): a) PVDF; b) PVDF-0.5 and c) PVDF-3.0.

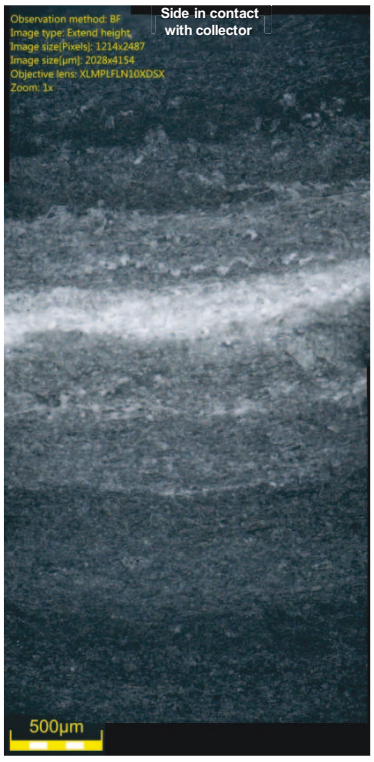

Figure 3. Optical image of the cross section surface in a sample of thirteen layers PVDF based material.

FSEM inspection was carried out in order to study the structure at submicrometric scale associated to the SBS PVDF-based materials as a function of the relative amount of MWCNT added. Images of cross-sectioned samples were taken (a razorblade was used to cut the samples under cryogenic conditions). Figure 4 shows a typical cross-section image at low magnification of one sample prepared by SBS (in particular neat PVDF). As can be seen, the whole cross-sectioned surface presents a fibrous morphology similar to that elsewhere described for the surface of similar material [18]. Figure 4b shows typical image at higher magnification of the morphology that can be observed in any region of the cross section depicted in Figure 4a.

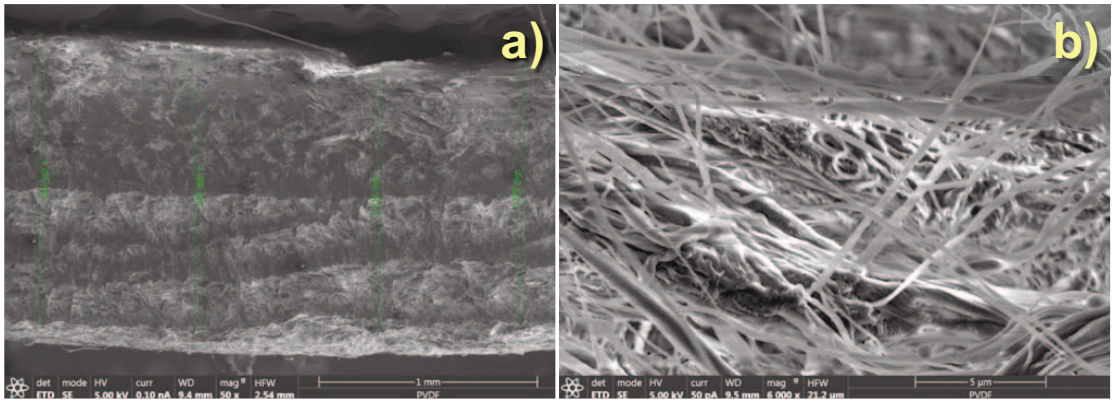

Figure 4. FSEM micrographs at (a) low and (b) high magnifications of a cross-sectioned sample of neat PVDF prepared by SBS.

On the other hand, in Figure 5 it is shown characteristic images at different positions from the surface (300, 700 and 1900 μm) along the cross-sectioned thirteen layers sample (following a direction perpendicular to the main plane of the SBS layers). In principle, from one of the surfaces to the center of the sample there should be a decrease in the concentration of MWCNT, therefore, it is expected to see for the images taken how the SBS PVDF morphology changes as the MWCNT concentration decreases.

In all cases fibers with diameters of around 350 nm are observed mixed with some random coils made of fibers with globular shape (pointed out with arrows in Figure 5). Regardless the region inspected it was always found that the number of random coils increased more at locations closer to the surface of the sample, suggesting that presence of carbon nanotubes induces variations in morphology, increasing the proportion of random coils as MWCNT concentration increases. These results corroborate that bulk morphology of SBS PVDF-based materials varies as a function of MWCNT concentration similarly to that observed in their corresponding surface [18]. An increase of viscosity, when the relative amount of MWCNT increases, seems to be the main factor influencing the morphology observed [18]. Higher viscosities should lead to slower displacement of the suspensions, favoring higher accumulation of material in the nozzle gate that finally can be sputtered to the collector.

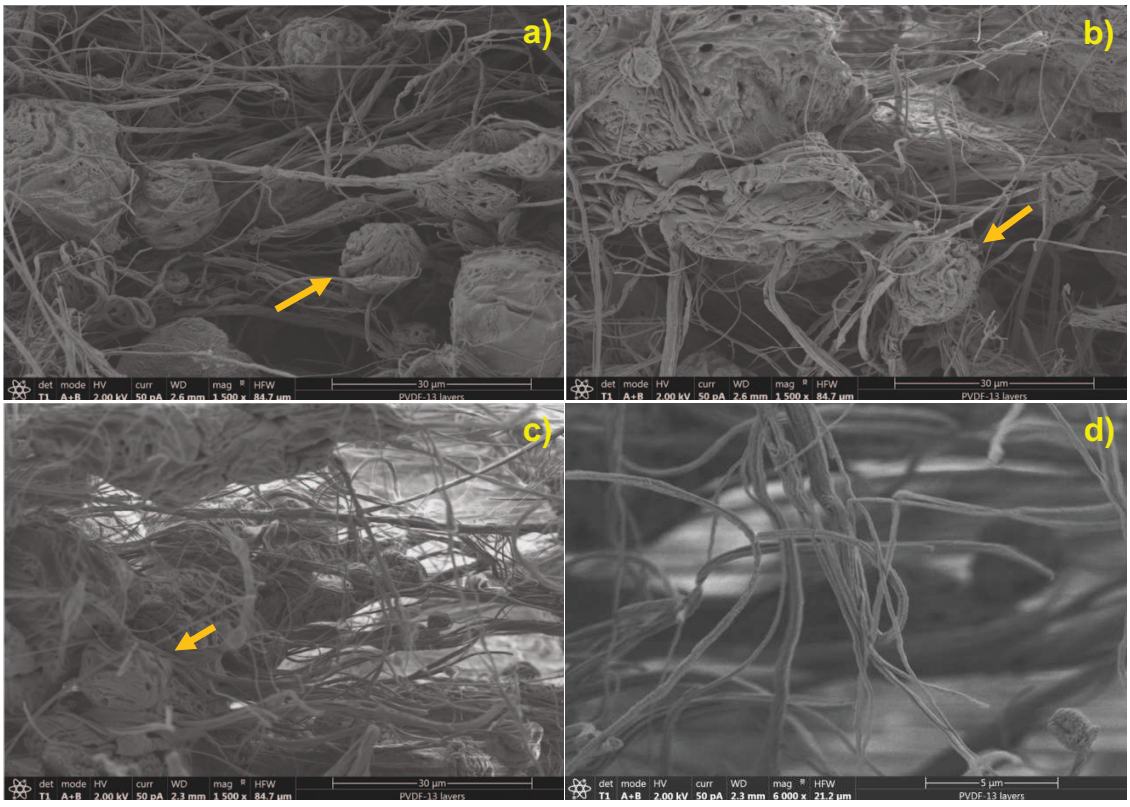

Figure 5. FSEM images at different positions from the surface: a) 300 µm; b) 700 µm; c) 1900 µm and d) 1900 µm (higher magnification) along the cross-sectioned thirteen layers sample.

Analysis of X-ray diffraction patterns is an effective way of identifying the presence of the different PVDF polymorphs [47–50]. However, still there is certain controversy about the real position of peaks to distinguish between the electroactive phases β and γ. In general, the appearance of intense peaks at 2θ = 18.4º and 20.0º and five weak peaks at 26.6, 33.2, 35.9, 38.8, and 41.1º corresponding to reflection of (020), (110), (021), (130), (200), (002), and (111) planes respectively would evidence the presence of the monoclinic α phase. However, as can be seen in Figure 6, all the materials prepared only show a shoulder at 18.4 º and a very weak signal at ~26.0º, indicating a very small contribution of α phase. On the other hand, the positions of the rest of peaks observed in Figure 6 at 20.5º, 25.8º, 36.2º and 40.7º suggest a mixture of β and γ phases. The broad peak at 20.5º might indicate the presence of β and γ phases, since (110) reflection of the monoclinic γ phase appears at 20.3º and (110)/(200) reflections of orthorhombic β-phase appear at 20.6º. The peak at 26º might be the consequence of a mixture of α and γ peaks; however, attending the small contribution of α phase it should mainly arise from the γ crystals. On the other hand, the peak at 36.2º might be the result of a combination of peaks arising from α and β phases; one at 35.9º associated to the (200) reflections in α phase and other at 36.5º corresponding to the (020) reflection of the β phase; however, again due to the small fraction of α phase, the peak at 36.2º should mainly belong to the β phase. Finally, the peak at 40.5º must mainly come from the reflection of the (211) planes in the γ phase.

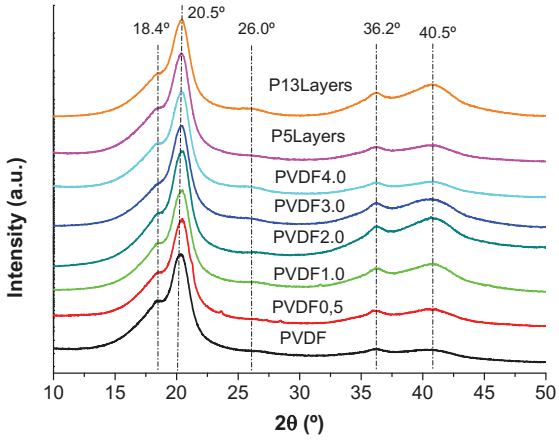

Figure 6. X-ray diffraction patterns obtained for all the samples under study.

Taking into account the small differences between X-ray diffraction patterns of α, β and γ phases it is really difficult to extract information about the relative contribution of the different phases; thus, FTIR spectroscopy has been used as a complementary technique. Depending on the experimental conditions, wavelength of infrared light, λ, and the angle of incidence of the IR beam relative to the surface of the ATR device crystal, θ, typical depth of penetration in ATR ranges from about 0.5 microns up to about 5 microns. Taking into account that porosity of similar samples prepared is slightly higher than 60 % [18], an estimated penetration in the porous materials up to 12.5 micrometers is expected and therefore, the information that can be extracted from the FTIR-ATR spectra must come exclusively from the layer directly in contact with the ATR crystal (thickness greater than 300 μm, see Figure 3). In Figure 7 the FTIR-ATR spectra are shown. In the high energy region, see Figure 7a, four main peaks can be observed. The peaks centered at 3018 cm^{-1} and 2978 cm^{-1} can be attributed to the C-H stretching vibrations of the methylene groups of the PVDF. The peaks centered at 2918 cm^{-1} and 2848 cm^{-1} only can be observed when MWCNT are added to the polymer, suggesting that they arise from C–H_x stretching vibrations of chemisorbed hydrogen as was reported for as-grow MWCNT samples [51].

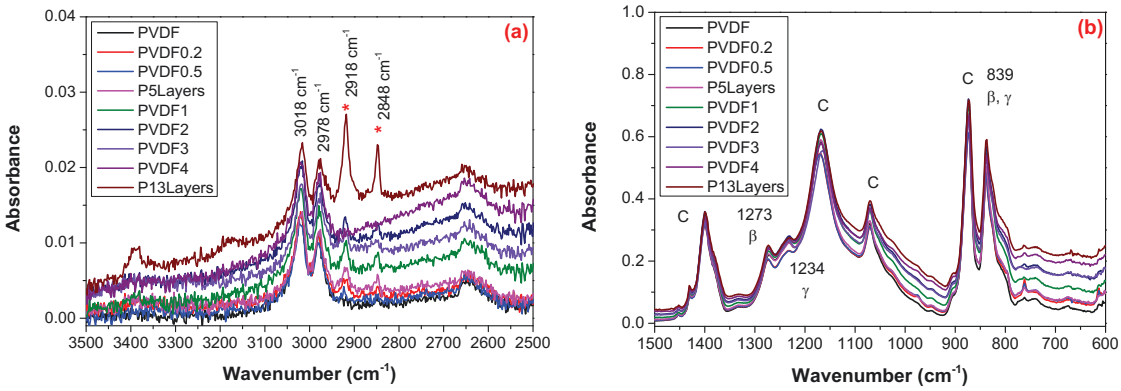

Figure 7. FTIR-ATR spectra of all the PVDF based materials prepared in this work.

The spectra of Figure 7b were labeled making use of the information available in the literature about the IR band assignation for the different structural conformations of the PVDF molecules associated with their main crystalline phases (α, β and γ) [18,26,47]. The letter C was used to point out common bands of PVDF that can be always found (880, 1072, 1172 and 1401 cm^{-1}) regardless the polymorphic form [47]. Although bands typically assigned to the α phase (614 cm^{-1} and 762 cm^{-1}) are observed, they are extremely

weak (Figure 7b). This result suggests therefore that α phase must have very small contribution. On the other hand, bands exclusively attributed to the β and γ phases appearing at 1273 cm^{-1} and 1234 cm^{-1} respectively can be clearly observed in Figure 7b while the band centered at 839 cm^{-1} might belong to both polymorphs β and γ. All these results confirm what was already stated when XRD measurements were discussed, solution blow spinning of PVDF based nanocomposites leads to materials for which the PVDF mainly crystallizes in the electroactive phases β and γ [18]. Following the method proposed by Cai et al [47] an estimation of the contributions of the three main phases identified in the IR spectra was done, and fractions of α, β and γ phases, F(α), F(β) and F(γ) respectively (eqs. 5, 6 and 7).

$$F(\alpha) = 1 - F_{EA} = 1 - \frac{A_{EA}}{\left(\frac{K_{839}}{K_{762}}\right)A_{762} + A_{EA}} \quad (5)$$

$$F(\beta) = F_{EA} \times \left(\frac{A_{\beta}}{A_{\beta} + A_{\gamma}}\right) \quad (6)$$

$$F(\gamma) = F_{EA} \times \left(\frac{A_{\gamma}}{A_{\beta} + A_{\gamma}}\right) \quad (7)$$

Where F_{EA}, is the fraction of electroactive phases β and γ, A_{EA} and A_{762} are the absorbances at 839 and 762 cm^{-1}, respectively, K_{839} and K_{762} are the corresponding absorption coefficients, 7.7×10^4 and 6.1×10^4 (cm^2/mol), respectively [52] and A_{β} and A_{γ} are the absorbances taken at the peaks associated to the β and γ phases at 1273 and 1234 cm^{-1} respectively (to take the absorbance values base line corrections were carried out in each band).

For every material prepared the fraction of the different PVDF polymorphs estimated from the FTIR-ATR results is gathered in Table 2.

Table 2. Fraction of the different PVDF polymorphs estimated from the FTIR-ATR results.

Sample	F(α)	F(β)	F(γ)
PVDF	0.10	0.58	0.32
PVDF-0.2	0.22	0.56	0.22

PVDF-0.5	0.15	0.63	0.22
PVDF-1.0	0.07	0.61	0.32
PVDF-2.0	0.07	0.62	0.31
PVDF-3.0	0.03	0.64	0.33
PVDF-4.0	0.09	0.63	0.28
P5Layers	0.10	0.61	0.29
P13Layers	0.07	0.67	0.25

It can be observed that, regardless the concentration of MWCNT, the main polymorph (with the highest contribution) is the β-phase, being in accordance with other works already published about similar systems [18]. On the other hand, the relative amount of both electroactive phases, β and γ does not seem to change largely with the concentration of MWCNT; perhaps there is a very slight increase of β phase when MWCNT is added to the PVDF as can be better seen for the P13Layers (Table 2). However, here it is important to highlight that this effect is simply an apparent effect since it would mainly arise from the contribution of the two outer layers respect to the whole material (13 layers).

In Figure 8 DSC curves of PVDF based materials obtained from a first heating and subsequent cooling and a heating after erasing the thermal and processing history are shown. During the first heating two endothermic thermal transitions are observed, one appearing within a range of 66.5 to 68.7 ºC, T_1, and the other one at about 167 ºC, T_2 (Figure 8a and Table 3). The first transition is not usually described for the PVDF and may be associated to a kind of relaxation due to the preferential orientation of macromolecules at the amorphous regions due to the formation of fibers by SBS. On the other hand, the second transition corresponds to the typical melting process of PVDF. In general, it is accepted that melting temperatures of PVDF α and β phases are very close each other, appearing in the range 162–172°C [52], therefore, structural information cannot be given from the analysis of these DSC curves. After erasing the thermal and processing histories during a cooling, one or two exothermic peaks can be observed depending on the sample (Figure 8b); one at lower temperature, T_{c1}, and the other at higher temperature T_{c2} (Table 3). As can be observed when MWCNT are present in the sample the peak at higher temperatures always appears. Furthermore, the higher the concentration of MWCNT the higher the temperature of that peak. These results point out a clear nucleation effect induced by the presence of nanoparticles (MWCNT) [39,53]. On the other hand, when there is enough difference of MWCNT concentration between layers

or, when a better defined interface is created, a double crystallization peak is observed (Samples PVDF1.0, PVDF2.0, PVDF3.0 and PVDF4.0). Finally, after erasing processing history and regardless the sample, the heating scan leads to only one endothermic peak at a slightly higher temperature, T_2' (170 ºC, Figure 8c and Table 3) than that obtained in the first heating, T_2. This result suggests that after melting the SBS materials and their subsequent crystallization at 10 ºC/min the PVDF based samples are mainly constituted by α phase which melts at slightly higher temperatures than the β-phase [18]. Besides, the first relaxation temperature disappeared confirming the removal of that order given by de SBS process.

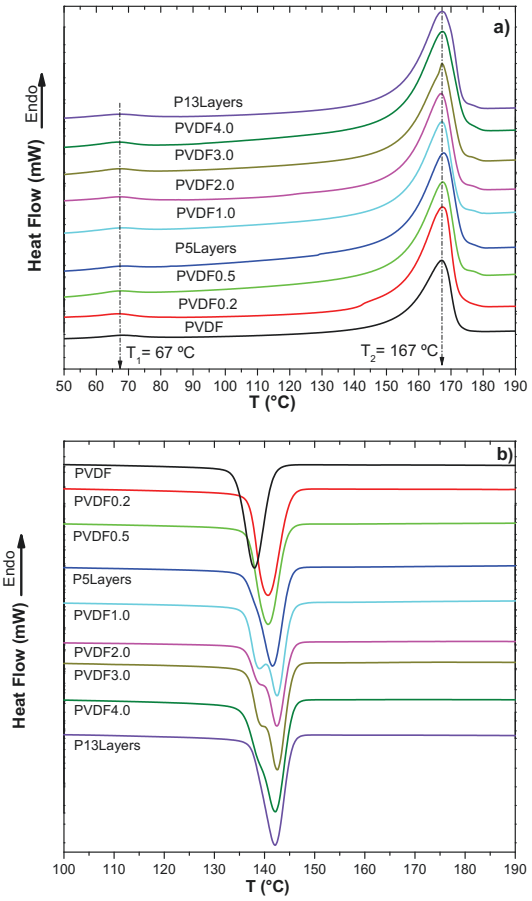

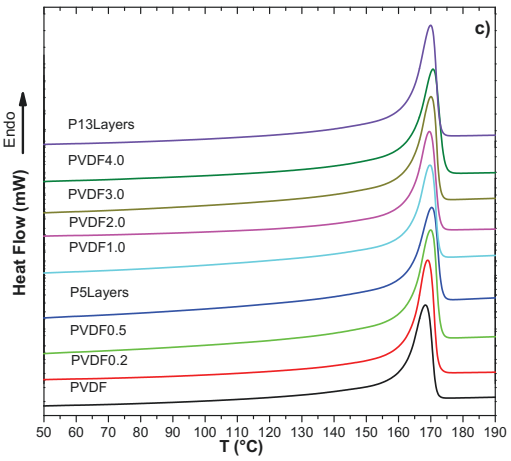

Figure 8. DCS curves of PVDF based materials obtained from a first heating (a) and a cooling (b) and heating after erasing the thermal and processing history (c).

Attending the crystallinity it is interesting to highlight that the presence of MWCNT slightly decreases the crystallinity degrees of the materials obtained from eqs. 1 (χ_m, χ_c and χ_m', Table 3 and Figure 9). A possible explanation of this result may be associated to the nucleation effect if the presence of higher relative amount of spherulites leads to higher fraction of interpherulitic amorphous phase. It is well known that crystalline fraction might influence final performance (electrical, thermal, mechanical, surface properties, etc.) of these kind of materials.

Table 3. Parameters obtained from the DSC curves of the PVDF based materials under study.

	1rst Heating			Cooling			2nd Heating	
Sample	**T_1 (ºC)**	**T_2 (ºC)**	**χ_m (%)**	**T_{c1} (ºC)**	**T_{c2} (ºC)**	**χ_c (%)**	**T_2' (ºC)**	**χ_m' (%)**
PVDF	68.4	167.2	63.1	138.0	-	50.8	168.4	54.5
PVDF-0.2	66.7	167.4	58.3	-	140.7	49.0	169.0	52.2
PVDF-0.5	67.9	167.4	56.5	-	140.7	48.5	169.9	51.9
PVDF-1.0	68.1	167.2	57.1	139.0	142.6	49.8	169.7	53.0
PVDF-2.0	67.0	166.9	58.1	139.1	142.4	48.5	169.5	51.1
PVDF-3.0	67.4	167.2	56.7	139.5	142.5	48.8	170.1	51.7
PVDF-4.0	66.4	167.5	52.0	139.0	142.1	44.3	170.7	47.6
P5Layers	68.7	167.7	60.0	-	141.5	50.4	170.2	53.6
P13Layers	67.9	167.3	57.4	-	142.2	49.2	170.1	53.0

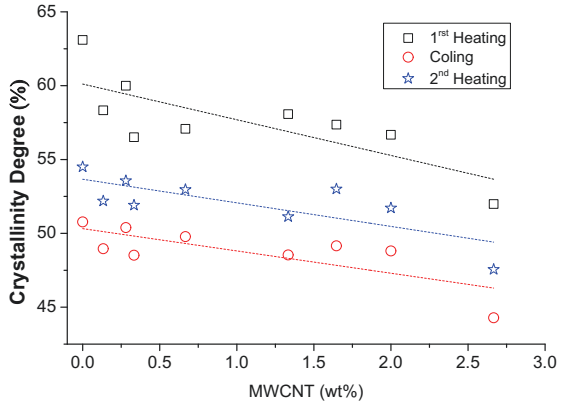

Figure 9. Crystallinity degree as a function of the weight percent of MWCNT.

Using the impedance data and equations 2, 3 and 4 it is possible to represent the real and imaginary parts of the permittivity, ε' (ability of the material to storage charge) and ε'' (loss of energy in the material) respectively, and the loss factor or dissipation factor, tan δ, as a function of frequency. A representative example is shown in Figure 10a where a characteristic result obtained from one measurement corresponding to the sample P13Layers is shown. The rest of samples lead to similar profiles, as comparison Figures 10b and 10c show representative plots of the real and imaginary parts of permittivity as a function of frequency for all the samples under study (a sample of pure PVDF obtained from hot pressing was also added).

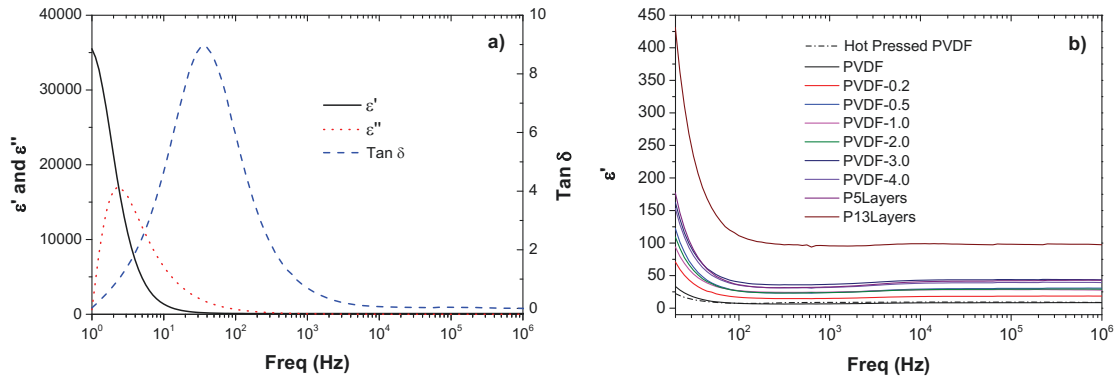

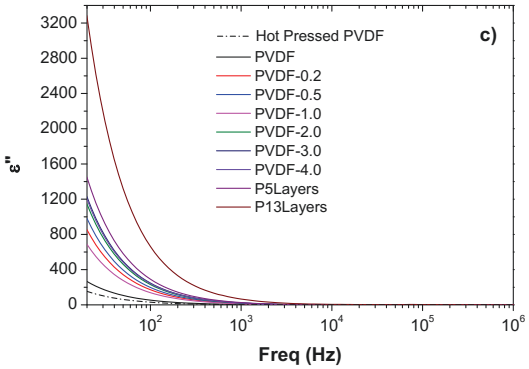

Figure 10. a) Real and imaginary parts of the permittivity, ε' and ε'' respectively, and dissipation factor, tan δ, as a function of frequency (representative result from one measurement corresponding to the sample P13Layers). b) and c) representatives plots of the real and imaginary parts of permittivity respectively as a function of frequency for all the samples under study.

It can be observed a loss peak at low frequencies. In general, at room temperature, relaxation phenomena appearing at frequencies below 50 Hz are usually attributed to space or interfacial charge polarization phenomena [1]. For the materials under consideration in this work, the relaxation observed might arise from the complex fibrous structure slightly enhanced in the case of nanocomposites due to the presence of nanofillers. Apart from that, here it is important to highlight that the values of the real and imaginary parts of the permittivity were indirectly obtained from equations 2 and 3 and they might fail at low frequencies. Other authors that also studied systems based on PVDF or PVDF-based copolymers [54,55] filled with carbon nanotubes did not observed the relaxation phenomenon described in the present work; however, they studied bulk samples without pores and, in addition to this, they directly measured the complex permittivity.

From plots like those given in Figure 10 (three frequency sweeps from three specimens per sample), averaged data were able to be obtained (Table 4). In particular, the relative permittivities at different frequencies were included in Table 4: i) the frequency associated to the space or interface charge polarization, f_m (maximum of the loss factor, tan δ); ii) 1 kHz, $f_{1\ kHz}$, and iii) 1 MHz, $f_{1\ MHz}$. Besides, the relaxation time, $1/f_m$, obtained from the frequency at the maxima of the loss factor, was also shown in Table 4.

It can be observed that permittivity value obtained for the neat PVDF prepared by SBS was similar to those found by other authors when the polymer is prepared by more conventional methods [1,13,56,57]. On the other hand, when MWCNT are added it is observed an increase of the permittivity that can be associated to the formation of a large number of nanocapacitors where interfacial polarization would happen, in other words where nomadic charges would pile up at the interface formed between the MWCNTs and the polymer matrix [56,58], this process of charge polarization is commonly known as Maxwell-Wagner-Sillars mechanism [59,60]. None correlation was observed between polymer structure, morphology and crystallinity and the permittivity, suggesting that they are not the main factors affecting the dielectric behavior of this kind of materials.

In the present work is shown for the first time the effect of a compositional gradient of a polymer composite material acting as the dielectric in a capacitor. First of all, lets us analyze dielectrics made by three SBS layers of PVDF based materials. As can be seen in Table 4 when increasing the concentration of MWCNT from 0.1 to 4 % by weight in the outer layers there is an increase of the permittivity which seems to remain constant when percolation fraction is reached below 3% by weight in the case of carbon nanotubes [58]. In principle, when reaching good conductivity for the outer layers passing through the percolation threshold one would expect to have again the permittivity of the neat PVDF since the outer layers might be considered a simple extension of the capacitor electrodes. However, the permittivity remained nearly constant with a value about 80% higher than that corresponding to the neat PVDF. This result might be explained considering that the outer layers in fact slightly penetrate the neat PVDF layer due to its porous nature leading to a thin region in-between the layers with a gradient of compositions due to the mixture between neat PVDF fibers and fibers of PVDF filled with MWCNT. Extending that gradient along the distance as can be represented by the samples with more than three layers, P5Layers and P13Layers, it is seen how it is possible to increase even more the permittivity for a certain frequency. Data obtained in nanotubes and graphene filled polymer composites point out increments in the real and imaginary parts of permittivity [60]. Therefore, attending the present results, again it seems to be confirmed that presence of conductive particles like MWCNT favors space charge polarization at the interface formed between the MWCNT and the polymer matrix. Furthermore, it can be also confirmed the existence of mainly one polarization mechanism

regardless the sample attending the same value found for the relaxation time (Table 4) associated to the process of polarization.

On the other hand, here it is interesting to highlight that the value of permittivity at 1kHz obtained for the material P5Layers (34.5) is relatively close to the value obtained from the sum of permittivities arising from the materials PVDF-0.2 and PVDF-0.5 (41.8) while, the value of permittivity at 1kHz obtained for the material P13Layers (90.7) is close the value obtained from the sum of permitivities arising from the materials PVDF-0.2, PVDF-0.5, PVDF-1.0 and PVDF-2.0 (94.3). These results suggest therefore that, at least in the case of PVDF/MWCNT system, there is a very easy way to design materials with tailored dielectric properties, simply overlapping layers of composite with different concentrations. Furthermore, the use of solution blow spinning allows preparing those materials very easily, with complex configurations and highly scalability.

Finally, it is well known that dielectric loss shows the ability of a dielectric to dissipate energy under an alternating field, and should be kept low for charge storage applications. Although in general, there is a small increase of dielectric loss (see the values of ε'' at 1kHz in Table 4) after adding MWCNT to the outer layers of the dielectrics it can be always considered low independently of the concentration of MWCNT. In principle, two possible contributions might account for the slight dielectric loss increase: i) the increase in the number of conductive particles that may enhance charge motion and ii) an increase of defects that should increase with the concentration of MWCNT and the thickness and number of layers. It seems that the second contribution plays a more important role since the sample P5Layers although having less concentration of MWCNT but more layers presents slightly higher losses than the samples, PVDF-1.0, PVDF-2.0, PVDF-3.0 and PVDF-4.0. Apart from the above mentioned the most important result is that always, regardless the sample studied in this work, the dielectric loss is very low. The reason is that actually, there is always a core in the dielectric mainly constituted by neat PVDF and there is always an important barrier for the charge carriers to move from one electrode of the capacitor to the other avoiding energy losses by charge leaking.

Another way of analyzing dielectrics in terms of their utility for charge storage applications is attaining low values of dissipation factor, tan δ, defined as the ratio of dielectric loss, imaginary part of the permittivity, over real part of the permittivity. For

all the systems under study, the values of tan δ were of about 0.7 in any case at a frequency of 1 kHz and less than 6.0 at 100 Hz. Therefore, it is confirmed that it is possible to increase the capacity to store electrical power (through higher values of permitivity) without altering energy losses, maintaining them very low.

Table 4. Averaged data of permittivity and relaxation time obtained from plots like those given in Figure 9.

Sample	ε' (at f_m)	ε' (at f_1 kHz)	ε' (at f_1 MHz)	ε'' (at f_1 kHz)	$(1/f_m)\times 10^2$ (s)
PVDF	12.8 ± 1.2	6.6 ± 0.3	8.4 ± 0.3	4.7 ± 0.1	2.4 ± 0.2
PVDF-0.2	30.2 ± 2.3	15.2 ± 1.1	19.0 ± 1.2	10.3 ± 0.3	2.6 ± 0.1
PVDF-0.5	50.6 ± 5.3	26.6 ± 1.9	34.1 ± 2.6	20.0 ± 1.9	2.3 ± 0.1
PVDF-1.0	44.3 ± 9.2	22 ± 3.8	25.6 ± 3.0	12.5 ± 0.2	2.8 ± 0.3
PVDF-2.0	56.4 ± 8.3	29.5 ± 4.3	35.9 ± 5.1	19.2 ± 3.2	2.5 ± 0.0
PVDF-3.0	67.2 ± 3.8	35.4 ± 1.5	42.3 ± 1.4	22.4 ± 0.3	2.6 ± 0.1
PVDF-4.0	63.7 ± 7.0	32.2 ± 2.5	39.4 ± 2.1	21.6 ± 0.6	2.5 ± 0.1
P5Layers	63.4 ± 5.9	34.5 ± 1.5	44.9 ± 1.7	27.3 ± 1.5	2.3 ± 0.2
P13Layers	188.5 ± 15.4	90.7 ± 3.8	96.0 ± 1.1	64.2 ± 2.1	2.7 ± 0.2

4. Conclusion

For the first time polymer based graded composites based on MWCNT filled PVDF were successfully prepared by solution blow spinning. There were morphology changes as a function of the concentration of MWCNT. Under the SBS conditions chosen the higher the concentration of MWCNT the higher amount of globular microstructures within a mainly fibrous morphology. Besides, the relative amount of both electroactive phases, β and γ increases very slightly with the concentration of MWCNT. However, these morphological and slight structural changes do not seem to be the main factor affecting the variations observed in the dielectric behavior of the materials under study. It was demonstrated that a particular design of PVDF based dielectrics where there is a particular gradient of MWCNT concentration importantly increases the permittivity without increasing dielectric losses. For example, in this particular work a material formed by 13 layers symmetrically distributed from the center of 7 MWCNT concentrations had a

permittivity 93% higher than that corresponding to a material formed by one layer of the neat PVDF. With these graded materials it is possible to increase and even tune the capacity to store electrical power maintaining energy losses very low.

Acknowledgments

The authors appreciate the financial support received from the Ministerio de Economía y Competitividad [MAT2014-59116-C2]; the Universidad Carlos III de Madrid due to Fondos de Investigación de Fco. Javier González Benito [2012/00130/004] and the strategic Action in Composites materials and interphases [2011/00287/002]. Finally, we greatly thank the help given by Dr. Gustavo González-Gaitano (Dept. Chemistry, University of Navarra) conducting an extraordinary work with FTIR spectroscopy.

5. References

[1] S.P. Pawar, M. Arjmand, P. Pötschke, B. Krause, D. Fischer, S. Bose, U. Sundararaj, Tuneable Dielectric Properties Derived from Nitrogen-Doped Carbon Nanotubes in PVDF-Based Nanocomposites, ACS Omega. 3 (2018) 9966–9980. doi:10.1021/acsomega.8b01239.

[2] J. Lu, C.P. Wong, Recent advances in high-k nanocomposite materials for embedded capacitor applications, IEEE Trans. Dielectr. Electr. Insul. 15 (2008) 1322–1328. doi:10.1109/TDEI.2008.4656240.

[3] R. Gregorio, M. Cestari, F.E. Bernardino, Dielectric Behavior of Thin-Films of Beta-PVDF/PZT and Beta-PVDF/BaTiO3 Composites, J. Mater. Sci. 31 (1996) 2925–2930. http://www.cheric.org/article/137138.

[4] D. Olmos, J.M. Martínez-Tarifa, G. González-Gaitano, J. González-Benito, Uniformly dispersed submicrometre BaTiO3 particles in PS based composites. Morphology, structure and dielectric properties, Polym. Test. 31 (2012) 1121–1130. doi:10.1016/j.polymertesting.2012.08.005.

[5] Y. Bai, Z.Y. Cheng, V. Bharti, H.S. Xu, Q.M. Zhang, High-dielectric-constant ceramic-powder polymer composites, Appl. Phys. Lett. 76 (2000) 3804–3806. doi:10.1063/1.126787.

[6] J. Lu, K.S. Moon, J. Xu, C.P. Wong, Synthesis and dielectric properties of novel

high-K polymer composites containing in-situ formed silver nanoparticles for embedded capacitor applications, J. Mater. Chem. 16 (2006) 1543–1548. doi:10.1039/b514182f.

[7] H.W. Choi, Y.W. Heo, J.H. Lee, J.J. Kim, H.Y. Lee, E.T. Park, Y.K. Chung, Effects of BaTiO3 on dielectric behavior of BaTiO 3-Ni-polymethyl methacrylate composites, Appl. Phys. Lett. 89 (2006) 19–22. doi:10.1063/1.2354425.

[8] J. González-Benito, D. Olmos, J.M. Martínez-Tarifa, G. González-Gaitano, F.A. Sánchez, PVDF/BaTiO 3 /carbon nanotubes ternary nanocomposites prepared by ball milling: Piezo and dielectric responses, J. Appl. Polym. Sci. 136 (2019) 1–14. doi:10.1002/app.47788.

[9] A.B. Da Silva, M. Arjmand, U. Sundararaj, R.E.S. Bretas, Novel composites of copper nanowire/PVDF with superior dielectric properties, Polymer (Guildf). 55 (2014) 226–234. doi:10.1016/j.polymer.2013.11.045.

[10] Z.M. Dang, J.K. Yuan, J.W. Zha, T. Zhou, S.T. Li, G.H. Hu, Fundamentals, processes and applications of high-permittivity polymer-matrix composites, Prog. Mater. Sci. 57 (2012) 660–723. doi:10.1016/j.pmatsci.2011.08.001.

[11] M. Arjmand, S. Sadeghi, M. Khajehpour, U. Sundararaj, Carbon nanotube/graphene nanoribbon/polyvinylidene fluoride hybrid nanocomposites: Rheological and dielectric properties, J. Phys. Chem. C. 121 (2017) 169–181. doi:10.1021/acs.jpcc.6b10741.

[12] B. Wang, Y. Jiao, A. Gu, G. Liang, L. Yuan, Dielectric properties and mechanism of composites by superposing expanded graphite/cyanate ester layer with carbon nanotube/cyanate ester layer, Compos. Sci. Technol. 91 (2014) 8–15. doi:10.1016/j.compscitech.2013.11.014.

[13] J. Zhu, J. Shen, S. Guo, H.J. Sue, Confined distribution of conductive particles in polyvinylidene fluoride-based multilayered dielectrics: Toward high permittivity and breakdown strength, Carbon N. Y. 84 (2015) 355–364. doi:10.1016/j.carbon.2014.12.031.

[14] B. Wang, L. Liu, L. Huang, L. Chi, G. Liang, L. Yuan, A. Gu, Fabrication and origin of high-k carbon nanotube/epoxy composites with low dielectric loss through layer-by-layer casting technique, Carbon N. Y. 85 (2015) 28–37. doi:10.1016/j.carbon.2014.12.062.

[15] H.C. Song, J.E. Zhou, D. Maurya, Y. Yan, Y.U. Wang, S. Priya, Compositionally

graded multilayer ceramic capacitors, Sci. Rep. 7 (2017) 1–12. doi:10.1038/s41598-017-12402-7.

[16] L.H.C.M. Eliton S. Medeiros, Gregory M. Glenn Artur P. Klamczynski, William J. Orts, Solution Blow Spinning: A New Method to Produce Micro- and Nanofibers from Polymer Solutions, J. Appl. Polym. Sci. 113 (2009) 2322–2330. doi:DOI 10.1002/app.30275.

[17] J. González-Benito, J. Teno, G. González-Gaitano, S. Xu, M.Y. Chiang, PVDF/TiO2 nanocomposites prepared by solution blow spinning: Surface properties and their relation with S. Mutans adhesion, Polym. Test. 58 (2017) 21–30. doi:10.1016/j.polymertesting.2016.12.005.

[18] J. González-Benito, D. Torres, C. Ballesteros, V.M. Ruiz, J. Teno, PVDF based nanocomposites produced by solution blow spinning, structure and morphology induced by the presence of MWCNT and their consequences on some properties, Colloid Polym. Sci. (2019). doi:10.1007/s00396-019-04530-5.

[19] J. Teno, G. González-Gaitano, J. González-Benito, Nanofibrous polysulfone/TiO2 nanocomposites: Surface properties and their relation with E. coli adhesion, J. Polym. Sci. Part B Polym. Phys. 55 (2017) 1575–1584. doi:10.1002/polb.24404.

[20] J.K.Y. Lee, N. Chen, S. Peng, L. Li, L. Tian, N. Thakor, S. Ramakrishna, Polymer-based composites by electrospinning: Preparation & functionalization with nanocarbons, Prog. Polym. Sci. 86 (2018) 40–84. doi:10.1016/j.progpolymsci.2018.07.002.

[21] T. Lei, Z. Xu, X. Cai, L. Xu, D. Sun, New Insight into Gap Electrospinning: Toward Meter-long Aligned Nanofibers, Langmuir. 34 (2018) 13788–13793. doi:10.1021/acs.langmuir.8b03114.

[22] J. Yan, M. Liu, Y.G. Jeong, W. Kang, L. Li, Y. Zhao, N. Deng, B. Cheng, G. Yang, Performance Enhancements in Poly(vinylidene fluoride)-based Piezoelectric Nanogenerators for Efficient Energy Harvesting, Nano Energy. 56 (2018) 662–692. doi:10.1016/j.nanoen.2018.12.010.

[23] Q.X. Chen, P. a Payne, Industrial applications of piezoelectric polymer transducers, Meas. Sci. Technol. 6 (1995) 249–267. doi:10.1088/0957-0233/6/3/001.

[24] R. Gregorio, R.C. Capitão, Morphology and phase transition of high melt temperature crystallized poly(vinylidene fluoride), J. Mater. Sci. 35 (2000) 299–

306. doi:10.1023/A:1004737000016.

[25] R. Gregorio, D.S. Borges, Effect of crystallization rate on the formation of the polymorphs of solution cast poly(vinylidene fluoride), Polymer (Guildf). 49 (2008) 4009–4016. doi:10.1016/j.polymer.2008.07.010.

[26] D. Olmos, F. Montero, G. González-Gaitano, J. González-Benito, Structure and morphology of composites based on polyvinylidene fluoride filled with BaTiO 3 submicrometer particles: Effect of processing and filler content, Polym. Compos. 34 (2013) 2094–2104. doi:10.1002/pc.22618.

[27] J.S. Nunes, A. Wu, J. Gomes, V. Sencadas, P.M. Vilarinho, S. Lanceros-Mendez, Relationship between the microstructure and the microscopic piezoelectric response of the alpha- and beta-phases of poly(vinylidene fluoride), Appl. Phys. a-Materials Sci. Process. 95 (2009) 875–880. doi:DOI 10.1007/s00339-009-5089-2.

[28] J. Gomes, J. Serrado Nunes, V. Sencadas, S. Lanceros-Mendez, Influence of the β-phase content and degree of crystallinity on the piezo- and ferroelectric properties of poly(vinylidene fluoride), Smart Mater. Struct. 19 (2010) 065010. doi:10.1088/0964-1726/19/6/065010.

[29] X.U. Yue, Z. Wei-tao, Y.U. Wen-xue, H.U. a Li-gui, Z. Yu-jie, Z. Zhu-di, Crystallization Behavior and Mechanical Properties of Poly (vinylidene fluoride)/ multi-walled Carbon Nanotube Nanocomposites, Chem. Res. Chinese Univ. 26 (2009) 491–495. http://www.cjcu.jlu.edu.cn/hxyj/CN/article/downloadArticleFile.do?attachType=PDF&id=12927.

[30] X.G. Tang, M. Hou, J. Zou, R. Truss, M. Yang, Z. Zhu, Toughening and reinforcement of poly(vinylidene fluoride) nanocomposites with “ bud-branched” nanotubes, Compos. Sci. Technol. 72 (2012) 263–268. doi:10.1016/j.compscitech.2011.11.011.

[31] S.M. Hong, S.S. Hwang, Physical Properties of Thin PVDF/MWNT (Multi-Walled Carbon Nanotube) Composite Films by Melt Blending, J. Nanosci. Nanotechnol. 8 (2008) 4860–4863. doi:DOI 10.1166/jnn.2008.IC49.

[32] D. Olmos, C. Domínguez, P.D. Castrillo, J. Gonzalez-Benito, Crystallization and final morphology of HDPE: Effect of the high energy ball milling and the presence of TiO2 nanoparticles, Polymer (Guildf). 50 (2009) 1732–1742. doi:10.1016/j.polymer.2009.02.011.

[33] F. a. Sánchez, M. Redondo, J. González-Benito, Influence of BaTiO\n 3\n submicrometric particles on the structure, morphology, and crystallization behavior of poly(vinylidene fluoride), J. Appl. Polym. Sci. 132 (2015) n/a-n/a. doi:10.1002/app.41497.

[34] E.-C. Chen, T.-M. Wu, Isothermal crystallization kinetics and thermal behavior of poly(□-caprolactone)/multi-walled carbon nanotube composites, Polym. Degrad. Stab. 92 (2007) 1009–1015. doi:10.1016/j.polymdegradstab.2007.02.019.

[35] J. Feng, J. Sui, W. Cai, J. Wan, A.N. Chakoli, Z. Gao, Preparation and characterization of magnetic multi-walled carbon nanotubes-poly(l-lactide) composite, Mater. Sci. Eng. B Solid-State Mater. Adv. Technol. 150 (2008) 208–212. doi:10.1016/j.mseb.2008.05.017.

[36] J.S. Lee, G.H. Kim, W.N. Kim, K.H. Oh, H.T. Kim, S.S. Hwang, S.M. Hong, Crystal Structure and Ferroelectric Properties of Poly(vinylidene fluoride)-Carbon nano tube Nanocomposite Film, Mol. Cryst. Liq. Cryst. 491 (2008) 247–254. doi:10.1080/15421400802330861.

[37] R.S. Linghao He, Qun Xu, Chengwu Hua, Effect of Multi-Walled Carbon Nanotubes on Crystallization, Thermal, and Mechanical Properties of Poly(vinylidene fluoride, Polym. Compos. 16 (2010) 921–927. doi:10.1002/pc.

[38] R.S. Linghao He, Jing Sun, Xiaoli Zheng, Qun Xu, Effect of Multiwalled Carbon Nanotubes on Crystallization Behavior of Poly(vinylidene fluoride) in Different Solvents, Polym. Polym. Compos. 21 (2010) 449–456. doi:10.1002/app.

[39] L. He, X. Zheng, Q. Xu, Modification of carbon nanotubes using poly(vinylidene fluoride) with assistance of supercritical carbon dioxide: the impact of solvent., J. Phys. Chem. B. 114 (2010) 5257–62. doi:10.1021/jp911621y.

[40] K.T. Lau, D. Hui, The revolutionary creation of new advanced materials—carbon nanotube composites, Compos. Part B Eng. 33 (2002) 263–277. doi:10.1016/S1359-8368(02)00012-4.

[41] F.A. Sanchez, J. González-Benito, PVDFBaTiO 3 /carbon nanotubes ternary nanocomposites: Effect of nanofillers and processing, Polym. Compos. 38 (2017) 227–235. doi:10.1002/pc.23579.

[42] L.H.C.M. E.S. Medeiros, G.M. Glenn, A.P. Klamczynski, W.J. Orts, Solution blow spinning: a new method to produce micro- and nanofibers from polymer solutions, J. Appl. Sci. 113 (2009) 2322–2330. doi:10.1002/app.30275.

[43] E.S. Medeiros, G.M. Glenn, A.P. Klamczynski, W.J. Orts, L.H.C. Mattoso, Solution Blow Spinning, US 8,641,960 B1, 2014.

[44] Y. Rosenberg, A. Siegmann, M. Narkis, S. Shkolnik, The sol/gel contribution to the behavior of γ-irradiated poly(vinylidene fluoride), J. Appl. Polym. Sci. 43 (1991) 535–541. doi:10.1002/app.1991.070430314.

[45] J. González-Benito, D. Olmos, J.M. Martínez-Tarifa, G. González-Gaitano, F.A. Sánchez, PVDF/BaTiO3/carbon nanotubes ternary nanocomposites prepared by ball milling: Piezo and dielectric responses, J. Appl. Polym. Sci. 47788 (2019) 1–14. doi:10.1002/app.47788.

[46] S.K. Tripathi, A. Gupta, M. Kumari, Studies on electrical conductivity and dielectric behaviour of PVdF-HFP-PMMA-NaI polymer blend electrolyte, Bull. Mater. Sci. 35 (2012) 969–975. doi:10.1007/s12034-012-0387-2.

[47] X. Cai, T. Lei, D. Sun, L. Lin, A critical analysis of the α, β and γ phases in poly(vinylidene fluoride) using FTIR, RSC Adv. 7 (2017) 15382–15389. doi:10.1039/C7RA01267E.

[48] T. Lei, X. Cai, X. Wang, L. Yu, X. Hu, G. Zheng, W. Lv, L. Wang, D. Wu, D. Sun, L. Lin, Spectroscopic evidence for a high fraction of ferroelectric phase induced in electrospun polyvinylidene fluoride fibers, RSC Adv. 3 (2013) 24952–24958. doi:10.1039/c3ra42622j.

[49] D.M. Esterly, B.J. Love, Phase transformation to β-poly(vinylidene fluoride) by milling, J. Polym. Sci. Part B Polym. Phys. (2004). doi:10.1002/polb.10613.

[50] X. Cai, X. Huang, Z. Zheng, J. Xu, X. Tang, T. Lei, Effect of Polyaniline (Emeraldine Base) Addition on α to β Phase Transformation in Electrospun PVDF Fibers, J. Macromol. Sci. Part B Phys. 56 (2017) 75–82. doi:10.1080/00222348.2016.1270730.

[51] A. Misra, P. Tyagi, P. Rai, D.S. Misra, FTIR Spectroscopy of Multiwalled Carbon Nanotubes: A Simple Approachto Study the Nitrogen Doping, J. Nanosci. Nanotechnol. 7 (2007) 1820–1823. doi:10.1166/jnn.2007.723.

[52] R. Gregorio,, M. Cestari, Effect of crystallization temperature on the crystalline phase content and morphology of poly(vinylidene fluoride), J. Polym. Sci. Part B Polym. Phys. 32 (1994) 859–870. doi:10.1002/polb.1994.090320509.

[53] L. He, J. Sun, X. Zheng, Q. Xu, R. Song, Effect of multiwalled carbon nanotubes on crystallization behavior of poly(vinylidene fluoride) in different solvents, J. Appl. Polym. Sci. 119 (2011) 1905–1913. doi:10.1002/app.32907.

[54] Y. Feng, W.L. Li, Y.F. Hou, Y. Yu, W.P. Cao, T.D. Zhang, W.D. Fei, Enhanced dielectric properties of PVDF-HFP/BaTiO3-nanowire composites induced by interfacial polarization and wire-shape, J. Mater. Chem. C. (2015). doi:10.1039/c4tc02183e.

[55] Y. Wang, C. Xing, J. Guan, Y. Li, Towards flexible Dielectric materials with high dielectric constant and low loss: PVDF Nanocomposites with both Homogenously dispersed CNTs and ionic liquids Nanodomains, Polymers (Basel). 9 (2017). doi:10.3390/polym9110562.

[56] M. Arjmand, U. Sundararaj, Impact of BaTiO 3 as insulative ferroelectric barrier on the broadband dielectric properties of MWCNT/PVDF nanocomposites, Polym. Compos. 37 (2016) 299–304. doi:10.1002/pc.23181.

[57] M. Yang, H. Zhao, D. He, J. Bai, Constructing a continuous amorphous carbon interlayer to enhance dielectric performance of carbon nanotubes/polyvinylidene fluoride nanocomposites, Carbon N. Y. 116 (2017) 94–102. doi:10.1016/j.carbon.2017.01.105.

[58] J. González-Benito, D. Torres, C. Ballesteros, V.M. Ruiz, J. Teno, PVDF based nanocomposites produced by solution blow spinning, structure and morphology induced by the presence of MWCNT and their consequences on some properties, Colloid Polym. Sci. (2019). doi:10.1007/s00396-019-04530-5.

[59] J.A. Puértolas, J.F. García-García, F.J. Pascual, J.M. González-Domínguez, M.T. Martínez, A. Ansón-Casaos, Dielectric behavior and electrical conductivity of PVDF filled with functionalized single-walled carbon nanotubes, Compos. Sci. Technol. 152 (2017) 263–274. doi:10.1016/j.compscitech.2017.09.016.

[60] X. Xia, Z. Zhong, G.J. Weng, Maxwell–Wagner–Sillars mechanism in the frequency dependence of electrical conductivity and dielectric permittivity of graphene-polymer nanocomposites, Mech. Mater. 109 (2017) 42–50. doi:10.1016/j.mechmat.2017.03.014.

Declaration of interests

 The authors declare that they have no known competing financial interests or personal relationships that could have appeared to influence the work reported in this paper.

☐The authors declare the following financial interests/personal relationships which may be considered as potential competing interests:

Author Contribution Statement

Víctor M. Ruiz

Performance of all experimental tests except DRX, data curation; formal analysis, discussion of the whole paper.

Rafael Sirera

Performance of DRX experiments, analysis of DRX data and interpretation of DRX results.

Juan M. Martínez

Performance of dielectric measurements, analysis of dielectric and interpretation of dielectric results.

Javier González-Benito

Conceptualization; Data curation (except DRX); Formal analysis; Funding acquisition; Investigation; Methodology; Project administration; Resources; Software; Supervision; Validation; Visualization; Writing – original draft; Writing – review & editing.